Drag Coefficient of Water Droplets

Approaching the Leading Edge of an Airfoil

Mario Vargas*
National Aeronautics and Space Administration
Glenn Research Center
Brook Park, Ohio, 44135

Suthyvann Sor†
Instituto Nacional de Técnica Aeroespacial
Madrid, Spain

Adelaida García Magariño‡
Instituto Nacional de Técnica Aeroespacial
Madrid, Spain

This work presents results of an experimental study on droplet deformation and breakup near the leading edge of an airfoil. The experiment was conducted in the rotating rig test cell at the Instituto Nacional de Técnica Aeroespacial (INTA) in Madrid, Spain. An airfoil model was placed at the end of the rotating arm and a monosize droplet generator produced droplets that fell from above, perpendicular to the path of the airfoil. The interaction between the droplets and the airfoil was captured with high speed imaging and allowed observation of droplet deformation and breakup as the droplet approached the airfoil near the stagnation line. Image processing software was used to measure the position of the droplet centroid, equivalent diameter, perimeter, area, and the major and minor axes of an ellipse superimposed over the deforming droplet. The horizontal and vertical displacement of each droplet against time was also measured, and the velocity, acceleration, Weber number, Bond number, Reynolds number, and the drag coefficients were calculated along the path of the droplet to the beginning of breakup. Results are presented and discussed for drag coefficients of droplets with diameters in the range of 300 to 1800 micrometers, and airfoil velocities of 50, 70 and 90 meters/second. The effect of droplet oscillation on the drag coefficient is discussed.

Nomenclature

avi	=	Audio video interleave movie format
c	=	Airfoil chord
C_d	=	Drag coefficient
D	=	Droplet diameter
DBKUP	=	Airfoil designation
f	=	Square wave frequency introduced by activating a piezoelectric transducer
INTA	=	Instituto Nacional de Técnica Aeroespacial
LED	=	Light Emitting Diode
PIV	=	Particle Image Velocimetry

* Aerospace Engineer, Icing Branch, 21000 Brookpark Road, Associate Fellow AIAA
† Jefe del Laboratorio de Técnicas Avanzadas de Experimentación, 28850 Torrejón de Ardoz
‡ Consultora INSA, 28850 Torrejón de Ardoz

Q = Water flow rate
Re = Reynolds number
SLD = Supercooled Large Droplets
V = Velocity
V_{Slip} = Slip Velocity, relative velocity between the droplet and the air: ($\mathbf{V}_{droplet}$ - $\mathbf{V}_{air}$)
We = Weber number

I. Introduction

Supercooled Large Droplet (SLD) breakup near the leading edge of large transport airfoils may alter the mass flux of water reaching the leading edge and be a factor that needs to be accounted for in the prediction of ice accretion formation in icing codes. Studies of droplet breakup can provide experimental data on droplet deformation and the sequence of steps that lead to droplet disintegration. They can indicate the location where droplet breakup is initiated and the size and shape of the pieces that may be carried away by the airflow as the droplet goes through the breakup process and disintegrates or impacts the surface of the airfoil. They provide an understanding of the physics involved in the process of deformation and breakup. They also allow measurement or calculation of the main parameters along the path of droplets as they deform and breakup or impact the airfoil.

Previous studies[1,2] measured the droplet horizontal and vertical displacement against time and calculated the velocity, acceleration, Weber number, Bond number, and Reynolds number along the path of the droplet as it approached the leading edge near the stagnation line. The studies also presented the sequence of droplet deformation that leads to the initiation of breakup. Those studies were carried out for an airfoil with a chord of 0.47 meters and droplet diameters up to 1800 μm and allowed defining the beginning of the actual droplet breakup as the point along the path at which the thickness of the droplet reaches a minimum. One of the parameters calculated but not reported in those studies was the drag coefficient along the path of the droplet from deformation to initiation of breakup.

This paper presents and discusses the drag coefficient results obtained during the droplet deformation and breakup experiments conducted in July of 2011 and November of 2012 in the rotating rig test cell at the Instituto Nacional de Técnica Aeroespacial (INTA) in Madrid, Spain. The experiments are part of an international space act agreement between NASA and INTA. The experiments were conducted on an airfoil with chord length of 0.71 meter placed at the end of an arm rotating about a central axis at speeds from 50 to 90 m/sec.. A high speed imaging system was used to capture the droplet deformation and breakup as the droplets approached the leading edge of the airfoil along the stagnation line (Figs. 1 and 2). From the imaging data, the drag coefficient was calculated along the path of the droplet. The behavior of the drag coefficient was studied against other important parameters measured and/or calculated.

The present work is a continuation and extension of previous research efforts to measure the important parameters involved in droplet deformation and breakup, to study the effect of airfoil size and to identify the mechanism of droplet breakup as droplets approach the leading edge of an airfoil along the stagnation line. The results will help determine if icing codes need to be modified to account for droplet deformation when the size of the droplets is in the SLD regime.

II. Experimental Setup

The experimental setup has four main elements: the rotating arm unit, the airfoil attached at the end of the arm, the monosize droplet generator and the high speed imaging system. Figure 1 shows the conceptual view of the experiment setup with all the elements except the high speed imaging system. Figure 2 shows the experimental setup components in the test cell before a run. The setup is identical to the one used in previous experiments[1,2,3].

A. Rotating Arm Unit

The rotating arm unit consists of a 5 kW electric motor mounted on a support structure that rests on a solid base attached to the floor (Fig. 2). The support structure is attached to the base through four slip ring vibration dampers. The motor is placed inside the support structure with the axle perpendicular to the horizontal plane and in the direction of the ceiling. A rotating arm is attached to the axle of the motor. The length of the arm measured from the center of the axle to the airfoil model attached at the end is 2.37 meters (93.3 inches). For balancing, vibration control and additional strength, a system of struts is mounted on the axle and opposite the arm location (Fig. 2). Accelerometers on the arm and the axle are used to monitor the arm vibrations. The revolutions per minute of the arm are measured using a light emitting diode (LED) optical system. A small reflecting tape mounted on the side of the airfoil reflects the light in each revolution. The reflected light is picked up by a detector placed next to the LED. Each time that the detector registers the reflected light from the LED one revolution of the arm is counted. The

control of the electric motor is located in the control room, a section of the test cell separated from the rotating rig by a safety glass window. The revolutions per minute of the arm can be adjusted to set the airfoil model at velocities from 0 to 90 m/sec at less than 1 m/sec intervals.

B. Airfoil Models

Three airfoils were used during the experiments. They have the same geometry but different chord size. They are a generic type of thick airfoil designated as DBKUP 001, DBKUP 002 and DBKUP 003 (Fig. 3). Table 1 lists the coordinates of the airfoil. This type of airfoil geometry was chosen for the experiment because it is a blunt shape that simulates a scaled version of the type of leading edge shape found on large transport airfoils. The chord sizes of the airfoils are 0.21meters (8.3 inches), 0.47 meters (18.5 inches) and 0.71 meters (30.0 inches) respectively. The airfoil geometry was the same as that used in previous experiments[1]. The results reported in this paper are only for the 0.710 meter chord airfoil.

C. Monosize Droplet Generator

Two droplet generators were used in the experiments: a TSI MDG-100 Monosize Droplet Generator and a custom-made droplet generator fabricated by INTA. The droplet generator (Figs. 2, 3) consists of a distilled water container, an electric pump, a power supply to drive the electric pump, a flow control valve, a frequency generator and the vibration head. The electric water pump delivers the water flow from the container to the vibration head. The high precision flow rate control valve with a manometer allows fine adjustment of the flow rate before the water reaches the vibration head. At the vibration head the water is forced through a small orifice (100 μm in diameter) and a jet is formed. A disturbance in the form of a square wave at the appropriate frequency is introduced by activating a piezoelectric transducer controlled with a BK Precision model 4011A frequency generator. The jet is unstable at resonant frequencies and breaks into uniform droplets. For a given orifice diameter, flow rate and excitation frequency the diameter of the generated droplets is given by the equation:

$$D_{(\mu m)} = 317\left[\frac{Q_{(cc/\min)}}{f_{(kHz)}}\right]^{/3} \tag{1}$$

where Q is the water flow rate in cubic centimeters per minute; f is the frequency in kilohertz; and D is the diameter of the droplets in μm. Prior to the experiments, the TSI MDG-100 monosize droplet generator was calibrated for orifices from 100 to 800 μm. It was not originally designed for orifice sizes larger than 100 μm but when tested with commercially available larger orifices it performed well and droplets sizes from 100 to 1800 μm can be generated.

The custom-made droplet generator (Fig. 4) operates on the same principle as the TSI-MDG-100: vibration of a laminar water jet at a chosen frequency generates the droplets. The water is held in the head of the generator (Fig. 4). The lower part of the head has the orifice. The upper part of the head is made of a metallic plate that acts as a diaphragm. The outside of the metallic plate has a rod attached to it. The other extreme of the rod is attached to an actuator. The actuator through the rod vibrates the plate at a chosen frequency. The vibration of the plate is transmitted to the water jet leaving the orifice, causing its breakup and formation of the droplets. Droplets of sizes up to 4000 μm can be generated.

D. High Speed Imaging System

The high speed imaging system consists of the high speed camera (Fig. 2), the camera software, the lens system and the lighting. The high speed camera used during the experiment was a Photron SA-5. The camera can capture images at rates from 1000 to 1,000,000 frames per second (fps). During the experiments frame rates of 50000, 75000, and 150000 fps were used with corresponding resolutions given in pixels for the horizontal and vertical directions: 192x512, 192x312 and 128x184. As the frame rate is increased, the resolution of the camera decreases. The camera has a maximum shutter speed of 1 microsecond (μs) at frames rates below 775,000 fps. The camera software employed for capturing the high speed image sequences is Photron's FASTCAM Viewer (PFV) and is part of the camera system. The same software was used for post-processing the image sequences to generate the movies for data analysis and to select the frames at which the droplet tracking was to begin and end.

During the experiment, one lens configuration was used for two magnifications of the droplet deformation and/or breakup. The lens configuration consisted of a 200mm Micro Nikkor lens with a 2x doubler added between the

camera and the 200mm lens to double the focal length. Two magnifications were achieved by placing the camera at two different distances from the location where the droplets were falling at 0.24 meters (9.25 inches) along the span of the airfoil. For the first magnification the distance was 0.91 meters (36 inches) and for the second the distance was 0.36 meters (14 inches). The lighting was designed to illuminate the droplets from behind to create a shadowgraph (black color of the droplets against a white-gray background). The light source was a 2000 watt Xenon light with a lens to focus the beam.

III. Test Procedure, Data Processing and Test Matrix

E. Test Procedure

Before a test run, the high speed camera system is aligned so that the line of sight of the lens is parallel to the direction along the span of the airfoil at the midpoint of the leading edge (stagnation line along the span). The rotating arm is set at the position where the falling droplets from the monosize droplet generator will just graze the leading edge. The airfoil is held at the same location during the whole alignment process. The camera is placed at the distance required by the optics to obtain the needed magnification and such that the center of the lens depth of field is at the location where the falling droplets graze the airfoil leading edge. The camera sits on a x-y positioning table that allows careful adjustments in either direction. A custom made adaptor, designed to hold a laser pointer so that the laser beam is aligned with the camera lens, is inserted into the camera lens housing. The camera position is adjusted so that the laser beam from the laser pointer is parallel to the span of the airfoil (grazing it). This ensures that the direction of the lens is parallel to the direction of the airfoil span.

The airfoil is moved from the alignment position and a ruler with the smallest subdivision of one millimeter is placed at the location where the droplets will graze the leading edge of the airfoil. The camera is focused on the ruler and the number of pixels per millimeter is recorded, since the number of pixels in the camera sensor and the field of view are known. This conversion is used during the data analysis to measure the droplet diameter. The monosize droplet generator controls are adjusted to produce the range of droplet sizes needed. The personnel withdraw to the control room, where they are able to observe the motion and operation of the rotating arm through a safety glass. The camera is controlled with software run on a laptop computer located in the control room. The software is used to start the camera and set the controlling parameters including frame rate and shutter speed, and allows writing information on each camera frame above the recorded image. The following information is recorded on each frame during the experiment: frame rate, time of recording, image resolution, frame number, lens configuration, date and time, arm velocity and target droplet size.

The rotating arm is set in motion at the rotational speed corresponding to the target velocity. When it reaches the target speed, the camera recording is started and maintained for three or more rotations depending on the amount of data wanted for a particular run. Once the recording is completed the rotating arm is brought to a stop. The high speed movie is analyzed with the camera software to determine the quality of the recording in each of the three or more passes of the airfoil. If the droplets are in focus, the back light is uniform and the image area covers the horizontal displacement of the droplets, the experiment moves to the next test point and the process is repeated.

F. Data Processing

The camera software was used to generate the clips and to change them from raw format to avi. The change in format from raw to avi was done without using any compression to avoid altering the data. To post process the droplet data from the clips, a data analysis program was developed[3]. The program has a digital image processing part and a calculation part. It reads the movie in avi format and converts each frame from grayscale to binary for image segmentation and tracking. The program is initialized with the following input: file name of the video clip, camera resolution, frame rate of the movie, chord length of the airfoil tested, assigned number of the droplet being tracked, frame number where the tracking begins and frame number where the tracking ends.

The frame numbers where the tracking begins and ends are selected from the movie clip with help of the camera software. The assigned number of the tracked droplet is obtained from the frame where the tracking begins. The program identifies the droplets in a given frame by numbering them from left to right. In each frame the digital image processing part of the program calculates and/or records the following parameters for the droplet being tracked: frame number, time with respect to the tracking frame, time with respect to the first frame of the movie, x coordinate of the centroid, y coordinate of the centroid, area, perimeter, major and minor axes of an ellipse superimposed on the droplet, equivalent diameter based on the measured area, equivalent diameter based on the volume for an oblate spheroid. The equivalent diameter based on the volume for an oblate spheroid is calculated using the major and minor axes of the superimposed ellipse assuming the droplet is an oblate spheroid asymmetric

about the major axis on the plane of observation, symmetric about the minor axis on the plane of observation and rotationally symmetric about the axis pointing in the direction that the droplet is moving toward the airfoil[4].

The diameter based on the volume of the oblate spheroid was used in all calculations. As long as the droplet remains an oblate spheroid with the symmetries mentioned above, this diameter should remain constant since the volume of the droplet does not change. The diameter based on the area of the droplet cross section varies since the area is the cross section of a 3D body changing in shape. In all the calculations presented in this paper that involve the diameter of the droplet, the diameter used was the one based on the volume of the oblate spheroid[4]:

$$D = \sqrt[3]{b^2 \cdot a} \tag{2}$$

where b is the height of the droplet and a the width.

The calculation part of the program uses the parameters measured in the image processing part to calculate the following parameters with respect to time: horizontal and vertical displacement, velocity of the droplet with respect to the airfoil (frame of reference at rest with respect to the airfoil with the origin at the stagnation point), position of the droplet with respect to the airfoil, slip velocity, acceleration, Weber number, Reynolds number, Bond number and drag coefficient.

For each frame where a droplet is being tracked, the program generates an image tiff file of the frame. In this image file the centroid and the superimposed ellipse are plotted. The program saves the tiff files in a separate folder. After each run, the tiff files are used in sequence to generate a movie. The movie is used to verify that the program is following the droplet (centroid location) correctly, and that the axis of the superimposed ellipse accurately measures the height and width of the droplet.

G. Test Matrix

The test matrix for the experiment was designed to setup the droplet generator for a chosen theoretical droplet diameter. At each droplet size, test points were set for airfoil velocities of 50, 70 and 90 meters per second. Frame rate values employed were 25000, 50000, 65100, 75000, 87000, 100000 and 150000 fps. A speed of 75000 fps was used most frequently because it was a middle point between a frame rate that allowed observation of the droplet breakup and a reasonable resolution of 192x312 pixels. Two camera magnifications were employed during the test. The larger magnification gave more detail but only allowed observation of the droplets over a very small distance. The smaller magnification allowed observation of the droplet over a larger distance, from no interaction with the airfoil, to beginning of deformation, deformation and breakup or impact with the airfoil.

IV. Data Analysis and Results

The drag coefficient is one of the parameters calculated from the high speed imaging tracking of the droplets. In this section the definition and calculation of the drag coefficient will be explained followed by discussion of the individual parameters employed in its calculation. A baseline case will be presented and discussed followed by cases for different droplet sizes and velocities.

A. Drag Coefficient

The following is the basic definition of the drag coefficient applied to a droplet:

$$C_d = \frac{m_d \cdot a_c}{\frac{1}{2} \cdot \rho_{air} V_{slip}^2 \cdot A_p}$$

where m_d is the mass of the droplet, a_c the acceleration of the droplet, ρ_{air} the density of the air, V_{slip} the slip velocity (velocity of the droplet respect the air) and A_p is the projected frontal area of the droplet.

The drag coefficient compares the inertial force exerted on the droplet by the pressure and viscous forces against the force that will be exerted on the droplet by the forward stagnation point pressure if it were to act uniformly over the projected frontal area of the droplet.

B. Frames of Reference

Two frames of reference were used in the analysis of the data: a frame of reference at rest with respect to the laboratory and a frame of reference at rest with respect to the airfoil. The frame of reference at rest with respect to

the airfoil is located at the stagnation point on the leading edge. The tracking of the droplet, the horizontal displacement, the vertical displacement, the velocity, the acceleration, the slip velocity, the Reynolds number, the Weber number and the Bond number were measured and/or calculated in the frame of reference at rest with respect to the laboratory. When presenting the data, the frame of reference with respect to the airfoil is also used. The Galilean transformation is used when moving the data from the frame of reference in the laboratory to the frame of reference on the airfoil. When presenting data from the frame of reference at rest with respect to the airfoil, a drawing of the airfoil is shown on the graph with the origin of the axis located at the stagnation point. The slip velocity, the acceleration, the Reynolds number, the Weber number, the Bond number and the dimensions of the droplet are the same in both frames of reference.

C. Mass of the Droplet m_d

The mass of the droplet is given by:

$$m_d = \rho_l \cdot \frac{\pi}{6} \cdot D^3$$

where ρ_l is the density of the water and D is the diameter of the original spherical droplet before it begins deforming. The mass of the droplet is conserved along its path up to the point where the breaking up of the droplet begins and starts losing mass by shearing[3].

The measurement of the droplet diameter is based on the volume of the oblate spheroid as explained in section F. This approach allows the measurement of the diameter in cases where there is an initial deformation of the droplet. The initial deformation may be caused by the natural vibration of the droplet as it falls vertically, or by the presence of a slip velocity at the location where the tracking of the droplet is initiated. The value of the diameter used in the calculations is the average taken over the first ten frames after the tracking begins.

D. Droplet Acceleration a_c

The acceleration of the droplet is calculated from the measured horizontal displacement of the droplet against time. The displacement of the droplet against time is measured during the tracking of the droplet. It is plotted against time and curve fitted with a function of the form:

$$x = x_0 + a_1 \cdot e^{a_2 \cdot t} + a_3 \cdot e^{a_4 \cdot t}$$

where x is the horizontal displacement, t the time and a_1, a_2, a_3 and a_4 are the curve fitting coefficients. The horizontal displacement is in the frame of reference at rest with respect to the laboratory.

The first derivative gives the velocity of the droplet in the frame of reference at rest with respect to the laboratory:

$$V_d = a_1 \cdot a_2 \cdot e^{a_2 \cdot t} + a_3 \cdot a_4 \cdot e^{a_4 \cdot t}$$

The derivative of the velocity gives the acceleration of the droplet. The acceleration of the droplet is the same whether the frame of reference is taken at rest with respect to the laboratory or with respect to the airfoil.

$$a_d = a_1 \cdot {a_2}^2 \cdot e^{a_2 \cdot t} + a_3 \cdot {a_4}^2 \cdot e^{a_4 \cdot t}$$

E. The Slip Velocity

The velocity of the droplet with respect to the air is called the slip velocity and is defined as:

$$V_{slip} = |V_d - V_{air}|$$

Where the V_d and V_{air} are the velocity of the droplet and the air with respect to a frame of reference at rest in the laboratory. The slip velocity has the same value if the velocity of the droplet and the velocity of the air are calculated in a frame of reference at rest with respect to the airfoil.

The velocity of the air is given by an empirical correlation obtained from PIV measurements conducted for each of the airfoils[5].

F. The Projected Area A_p

For a droplet deforming along its trajectory the projected area A_p is given by:

$$A_p = \frac{l(t)^2}{4} \cdot \pi$$

where *l(t)* is the height of the droplet.

The width and height of the droplet are measured during the tracking of the droplet. At each frame the program measures the location of the centroid and superimposes an ellipse over the droplet. The program records the location of the centroid, the length of the two axes of the superimposed ellipse and its inclination with respect to the horizontal axis. The two axes of the ellipse correspond to the height and width of the droplet. For each frame, the program sends to a separate folder an image tiff file that is a copy of the frame with the location of the centroid and the superimposed ellipse plotted over it. After the tracking of the droplet is completed, the tiff files are used to create a QuickTime movie. The movie allows visual confirmation that the tracking is being done correctly and that the ellipse is giving the correct values of the width and height of the droplet. Figure 5 shows a few selected frames of a QuickTime movie merged into a single image for illustration of the droplet, the superimposed ellipse and the location of the centroid.

The major axis of the superimposed ellipse corresponds to *l(t)* and is used to calculate the projected area of the deformed droplet. The droplet is assumed to be rotationally symmetric along an axis directed along its direction of motion with respect to the airfoil frame of reference.

G. Calculated Drag Coefficient at a given Location Along the Path of the Droplet

The calculated drag coefficient of the droplet at a given location along its path is given by:

$$C_D = \frac{4}{3} \cdot \left(\frac{\rho_l}{\rho_a}\right) \cdot \left(\frac{D^3}{l(t)^2}\right) \cdot \frac{1}{\left(V_{slip}(t)\right)^2} \cdot \left[a_1 \cdot a_2^2 \cdot e^{a_2 \cdot t} + a_3 \cdot a_4^2 \cdot e^{a_4 \cdot t}\right]$$

where ρ_l and ρ_a are the water and air densities respectively. D is the droplet diameter. *l(t)* is the height of the droplet. $V_{slip}(t)$ is the slip velocity. *l* and V_{slip} vary with time as the droplet moves and deforms along its path and it is indicated by the time in parentheses written with their symbols. a_1, a_2, a_3 and a_4 are the curve fit coefficients.

The drag coefficient calculated above is based on its fundamental definition. In studies of droplet breakup where it was difficult or not possible to calculate the droplet deformation, researchers have used an alternative definition. They calculate the drag coefficient using the projected area of the spherical droplet before any deformation begins. The projected area used in the calculation remains constant and equal to $(\pi/4)*D^2$. This alternative way of calculating the drag coefficient is used in this paper for comparison purposes with the fundamental one. To differentiate this drag coefficient from the fundamental one its symbol is written $C_{Dsphere}$. In terms of the previous parameters $C_{Dsphere}$ is given by:

$$C_{Dsphere} = \frac{4}{3} \cdot \left(\frac{\rho_l}{\rho_a}\right) \cdot \frac{D}{\left(V_{slip}(t)\right)^2} \cdot \left[a_1 \cdot a_2^2 \cdot e^{a_2 \cdot t} + a_3 \cdot a_4^2 \cdot e^{a_4 \cdot t}\right]$$

$C_{Dsphere}$ is the drag coefficient for a non-deforming spherical droplet subject to the same inertial force and stagnation pressure as the deforming droplet being tracked. The flow field in this case is unsteady because the droplet is being continuously decelerated along its path.

For a solid sphere in steady state flow there is a classical correlation of drag coefficient against the Reynolds number[7]. For comparison purposes with C_D and $C_{Dsphere}$ this drag coefficient is also calculated and plotted with the other two in some of the figures. To differentiate it from the other two it is labeled $C_{Dsteady}$.

H. The Length Scale used in the Calculation of the Reynolds Number

When calculating the Reynolds number a length scale is employed. When a droplet is not deforming the diameter of the droplet is the proper length scale. When the droplet is deforming, the height of the droplet is the

proper length scale. The original diameter of the droplet, when the droplet is still spherical and before deformation begins could also be used. For the deforming droplet, when comparing drag coefficients against the Reynolds number in a plot, either Reynolds number may be employed.

I. Base Case

The Base Case, listed in Table I as 072011-11.5_Drop#1, is representative of the drag coefficient behavior observed for droplets from 300 to 1800 micrometers. Figure 6 shows the horizontal displacement against time and the curve fitting equation. On figure 7 the drag coefficients C_D and $C_{Dsphere}$ are shown against time. The drag coefficient for the deforming droplet, C_D, begins at 1.12 and decreases to a minimum value of 0.38 before increasing. After reaching a value of 0.58 it begins decreasing again. The final value measured is 0.38. The drag coefficient $C_{Dsphere}$ for the case of a non-deforming spherical droplet subject to the same inertial force and stagnation point pressure is also plotted in figure 7. $C_{Dsphere}$ and C_D begin at the same value and slowly depart from each other as long as the shape of the deforming droplet is not too far from spherical and the projected areas remaining close in value with the value of C_D being lower than the value of $C_{Dsphere}$. The values of C_D and $C_{Dsphere}$ gradually decrease to a minimum. After reaching the minimum value, $C_{Dsphere}$ increases more rapidly than C_D. The projected frontal areas differ more and more and the values of the drag coefficient are no longer close. The value of $C_{Dsphere}$ increases continuously to a maximum of 1.90 while the value of C_D shows an initial increase to a maxima and then decreases. The difference in behavior between the two drag coefficients shows the effect of the deformation of the droplet through the change in the projected area.

In figure 8 the drag coefficients C_D, $C_{Dsphere}$ are plotted against the Reynolds number together with the classical value of $C_{DSteady}$, the drag coefficient for a solid sphere in steady state flow. There are two plots for C_D. C_D is plotted in red for the case where the Reynolds number is calculated using the original diameter of the droplet. C_D is plotted in blue for the case where the Reynolds number is calculated based on the changing droplet height. For a Reynolds number range from 450 to 1100 the shape of the deforming droplet is not too far from spherical. Comparing C_D and $C_{DSteady}$ in this range, the values behave differently. Although in this range the shape of the deforming droplet is close to spherical, the value of its drag coefficients differ substantially from the classic value for a solid sphere. The difference can be attributed to the fact that the droplet is being decelerated and the flow field around the droplet is non-steady.

J. Drag Coefficient for Drops moving with respect to the Airfoil with an Initial Velocity of 90 m/sec

Figure 9 shows C_D and $C_{Dsphere}$ against time for a droplet with a diameter of 574 μm. The two drag coefficient remain close in value until a time of 1500 microseconds then $C_{Dsphere}$ increases faster than C_D to a value larger than one. The largest value of C_D before the droplet begins to breakup is less than one. Figure 10 shows C_D and $C_{Dsphere}$ against time for a droplet with a diameter of 1013 μm. The behavior of C_D and $C_{Dsphere}$ is similar to the base case discussed in section I. Figure 11 shows the two drag coefficients against time for a droplet with a diameter of 1271μm. The behavior of the two drag coefficients tends to follow the same pattern as the base case but with some differences. During the time that the shape of the droplet is still close to spherical, the differences between the two drag coefficients is more marked. Figure 12 shows the two drag coefficients against time for a droplet with a diameter of 1747 μm. The behavior of the two drag coefficients is markedly different from the base case discussed in section I. The two drag coefficients initially increase with values close to each other. Between 500 to 1300 microseconds, C_D is larger than $C_{Dsphere}$. C_D reaches a maximum value at 1300 microseconds and begins decreasing. $C_{Dsphere}$ continuously increases and after 1300 microseconds its value is larger than C_D. The behavior of C_D is due to the oscillation of the droplet before feeling the effect of the approaching airfoil. The oscillation of the droplet can be detected plotting the height, the width and the initial value of the droplet diameter against time. This is shown in Figure 13. The droplet height rapidly decreases to a value less than the initial diameter. It remains in this condition between the times of 500 to 1300 microseconds. Going back to figure 12 it can be seen that it is during this time that C_D is larger than $C_{Dsphere}$.

When the droplets are ejected from the generator they leave at a constant vertical velocity. The velocity is determined by the settings on the generator (pressure, discharge). The velocity can be as high as 10m/sec. The droplets travel nearly 8 inches before they enter the field of view of the camera where they are tracked. During that time the droplets may experience oscillations. The susceptibility of a droplet to oscillate increases with its diameter. Droplets with diameters larger than 1000 μm are more prone to oscillation. If the droplet is oscillating when the tracking begins the drag coefficient is affected and its behavior against time departs from the base case. Comparing the behavior of the height of the droplet against the original diameter indicates when the droplet is oscillating and affecting the measurement of the drag coefficient.

K. Drag Coefficient for Drops moving with respect to the Airfoil with an Initial Velocity of 70 m/sec

Figure 14 shows C_D and $C_{Dsphere}$ against time for a droplet with a diameter of 321μm approaching the airfoil at 70 m/sec. C_D and $C_{Dsphere}$ are close in value and slowly decrease to a minimum. $C_{Dsphere}$ remains slightly larger than C_D the whole time. The drag coefficients approach the 0.4 value from the classical correlation for a solid sphere in uniform flow. The behavior of the drag coefficients reflects the higher resistance to deformation observed in small droplets approaching the airfoil. The smaller radius of curvature of the droplets allows the surface tension force to resist the viscous and pressure forces trying to deform them. Larger drops with their larger radius of curvature generate a lower surface tension force to oppose the drag forces and are subject to more deformation. The C_D values are scattered in a band 0.2 wide. They have been curve fitted with a second order polynomial.

Figure 15 shows the two drag coefficients for a 720 μm drop. The two drag coefficient values tend to converge to the same value at the minimum. After reaching the minimum value, $C_{Dsphere}$ increases while the value of C_D remains flat at 0.4. Figures 16 and 17 show the two drag coefficients for drops of diameters 1096 and 1308μm. The behavior of the drag coefficient for the 1096 μm droplet is similar to the 720 μm case but after the minimum the value of C_D increases. The drag coefficients for the 1308 μm droplet behave similar to the base case. This is a large droplet but it does not exhibit oscillation.

L. Drag Coefficient for Drops moving with respect to the Airfoil with an Initial Velocity of 50 m/sec

Figure 18 shows C_D and $C_{Dsphere}$ against time for a droplet with a diameter of 375 μm approaching the airfoil at 50 m/sec. The C_D values are scattered in a band 0.2 wide, similar to what was observed in figure 14 for a 321 μm droplet at 70 m/sec. The scattering is caused by the uncertainty in the measurement of the diameter of the droplet due to the limit of the imaging system resolution. At the resolution of 14.26 pixel per millimeter, a droplet with a diameter of 375 μm spans about 5 pixels. Due to the discreetness of the camera sensor and the difficulty in resolving between the background pixels and the droplet pixels, an error of at least plus or minus 1 pixel can be incurred. This is an error of plus or minus 20%. For a drag coefficient value of 0.5 this translates to an error of plus or minus 0.1, an error band of 0.2.

Figure 19 shows the drag coefficients for a droplet with a diameter of 779 μm. The two drag coefficients remain very close in value during the whole path of the droplet. The overall pattern follows the base case. Figure 20 shows the drag coefficients for a droplet with a diameter of 1270 μm. The drag coefficients tend to follow the pattern observed in the base case but there is more separation in their values. Figure 21 shows the drag coefficients for a droplet with a diameter of 1433 μm. Between 200 and 1100 microseconds the value of CD is greater than the value of CDsphere indicating that the droplet was oscillating.

V. Conclusions

The behavior of the drag coefficient is highly non-linear for a deforming droplet approaching the leading edge along the stagnation line. The drag coefficient is determined by the acceleration of the droplet, the stagnation point pressure and the projected frontal area. At a given location along its path, the shape (geometry) and the flow field around the droplet will induce pressure and viscous drag forces that decelerate the droplet and distort its shape increasing the projected frontal area. As the droplet acceleration, shape and location change, its velocity, the velocity of the air and the flow field around the droplet change. The change in the flow field changes the stagnation point pressure. This new droplet shape and flow field will in turn modify the pressure and viscous forces acting on the droplet repeating the cycle of change in the acceleration, shape modification and change of the stagnation point pressure value. A subset of the data from the 2011and 2012 droplet breakup experiment conducted in the rotating rig test cell at the Instituto Nacional de Técnica Aeroespacial (INTA) in Madrid, Spain, was analyzed and the drag coefficients were calculated. The diameter of the droplets analyzed ranged from 300 μm to 1800 μm. The data presented is for an airfoil with a chord of 0.710 meters. The airfoil velocities were 50, 70 and 90 m/sec. From the analysis of the data the following conclusions can be stated:

- The drag coefficient calculated based on the original diameter of a droplet (constant frontal projected area) and the drag coefficient based on the varying droplet height (varying frontal projected area) follow a general pattern. As the deformation of the droplet is not too far from spherical the two drag coefficients remain close in value and decrease to a minimum. After reaching the minimum value the two drag coefficients increase. The drag coefficient based on the constant droplet diameter increases rapidly and reaches values greater than

one. The maximum value measured is 5.6. The value of the drag coefficient based on the varying droplet height always remains below 1.0.

- When droplet oscillation is present it has a strong effect on the value of the drag coefficient based on the varying height of the drop. During the oscillation, the height of the varying projected area of the droplet can become smaller than the projected are of the spherical droplet and its value will become larger than the drag coefficient based on the constant diameter of the initial spherical drop. In this case the drag coefficients will not follow the general pattern observed when the oscillation is not present.
- Comparison of the drag coefficient based on the droplet constant diameter, $C_{Dsphere}$, the drag coefficient based on the droplet varying height, C_D, and the classical value of the drag coefficient for a solid sphere, $C_{Dsteady}$, against the Reynolds number, showed that even during the time that the droplet deformation is not too far away from spherical, $C_{Dsphere}$ and C_D do not follow the classical correlation for $C_{Dsteady}$. This can be attributed to the deceleration that the droplet experiences which creates a non-steady flow field around it. For the smaller droplets tested, in the range of 300 μm, the effect was less marked.
- When water droplets are approaching the leading edge of an airfoil, they experience deceleration and deformation. This affects the drag coefficient of the droplets. The drag coefficient for droplets between 300 to 1800 μm , based on the constant droplet diameter or the varying droplet height, was markedly different from the classical value of the drag coefficient for a solid sphere in steady flow measured at the same Reynolds number.

The results of the work presented here will help in the development of improved ice accretion codes. The results also indicate the need for additional research work to better understand the physics involved in water drops deceleration and deformation as they approach the leading edge of an airfoil and its effect on the drag coefficient.

Acknowledgments

The authors would like to thank Mr. Chris Lynch for his excellent imaging work during the experiment. Thanks to Dr. Peter Struk for reviewing the paper. Thanks also to Mr. Yago Sánchez and Mr. Carlos Molina from ALAVA INGENIEROS for their support and expertise during the experiment. Thanks to all rotating rig INTA personnel for their excellent support in the preparation work and during the execution of the test program. The present work is part of the NASA/INTA collaboration under a Space Act Agreement. It is funded by the Atmospheric Environment Safety Technologies (AEST) Project, Aviation Safety Program (AvSP). Special thanks to Dr. Ron Colantonio for his support of the effort.

References

[1] Vargas, M. and Feo, A., ".Experimental Observations on the Deformation and Breakup of Water Droplets near the Leading Edge of an Airfoil," NASA/TM-2011-216946, AIAA Paper 2010-7670, August 2010.

[2] Feo, A., Vargas, M., and Sor, S., "Rotating Rig Development for Droplet Deformation/Breakup and Impact Induced by Aerodynamic Surfaces," SAE Technical Paper 2011-38-0087, 2011, doi:10.4271/2011-38-0087.

[3] Vargas, M., Sor ,S., García-Magariño, A., "Mechanism of Water Droplet Breakup near the Leading Edge of an Airfoil", AIAA Paper 2012-3129, June 2012.

[4] Sor, S., García-Magariño, A., "Diameter and Axisymmetry Measurements of a Water Droplet Impinging on an Airfoil", INTA Document No. AE-1NO-4420-065, March 2012.

[5] Sor, S., Personal communication on PIV data obtained at the INTA's Rotating Rig Facility

[6] Otsu, N., "A Threshold Selection Method from Gray-Level Histograms," IEEE Transactions on Systems, Man, and Cybernetics, Vol. 9, No. 1, pp. 62-66, 1979.

[7] Almedeij, J., "Drag Coefficient of Flow around a Sphere: Matching Asymptotically the Wide Trend," Powder Technology, Vol. 186, pp. 218-223, 2008.

Table 1. DBKUP Airfoil Coordinates

X-Coordinate	Y-Coordinate	X-Coordinate	Y-Coordinate
1.0000	0.0000	0.0000	0.0000
0.9989	-0.0009	0.0011	0.0139
0.9957	-0.0014	0.0043	0.0310
0.9904	-0.0025	0.0096	0.0498
0.9830	-0.0042	0.0170	0.0674
0.9735	-0.0064	0.0265	0.0842
0.9619	-0.0089	0.0381	0.1007
0.9484	-0.0120	0.0516	0.1170
0.9330	-0.0155	0.0670	0.1318
0.9157	-0.0195	0.0843	0.1458
0.8967	-0.0240	0.1033	0.1584
0.8759	-0.0291	0.1241	0.1700
0.8536	-0.0347	0.1465	0.1797
0.8297	-0.0410	0.1703	0.1880
0.8044	-0.0479	0.1956	0.1943
0.7778	-0.0554	0.2222	0.1985
0.7500	-0.0634	0.2500	0.2007
0.7211	-0.0721	0.2789	0.2006
0.6913	-0.0815	0.3087	0.1985
0.6607	-0.0915	0.3393	0.1938
0.6294	-0.1019	0.3706	0.1870
0.5976	-0.1128	0.4025	0.1780
0.5653	-0.1240	0.4347	0.1683
0.5327	-0.1353	0.4673	0.1577
0.5000	-0.1466	0.5000	0.1466
0.4673	-0.1577	0.5327	0.1353
0.4347	-0.1683	0.5653	0.1240
0.4025	-0.1780	0.5976	0.1128
0.3706	-0.1870	0.6294	0.1019
0.3393	-0.1938	0.6607	0.0915
0.3087	-0.1985	0.6913	0.0815
0.2789	-0.2006	0.7211	0.0721
0.2500	-0.2007	0.7500	0.0634
0.2222	-0.1985	0.7778	0.0554
0.1956	-0.1943	0.8044	0.0479
0.1703	-0.1880	0.8297	0.0410
0.1465	-0.1797	0.8536	0.0347
0.1241	-0.1700	0.8759	0.0291
0.1033	-0.1584	0.8967	0.0240
0.0843	-0.1458	0.9157	0.0195
0.0670	-0.1318	0.9330	0.0155
0.0516	-0.1170	0.9484	0.0120
0.0381	-0.1007	0.9619	0.0089
0.0265	-0.0842	0.9735	0.0064
0.0170	-0.0674	0.9830	0.0042
0.0096	-0.0498	0.9904	0.0025
0.0043	-0.0310	0.9957	0.0014
0.0011	-0.0139	0.9989	0.0009
0.0000	0.0000	1.0000	0.0000

Table 2. Test Conditions for Droplets Analyzed

Airfoil DBKUP 001 – Chord Size 0.710 meters

Run Number	Orifice µm	Droplet Theoretical Diameter µm	Airfoil Model Velocity m/sec	Magnification	Resolution H x V pixels / pixels per mm	Frame Rate Frames/sec
072011.11	200	400	80	1	192 x 312/14.26	75,000
072611.18	400	800	90	1/1	256x312/14.26	75,000
072011.13A	200	400	90	1	192 x 312/14.26	75,000
072611.16	500	1000	90	1/1	192x312/14.26	75,000
072611.15B	700	1400	90	1/1	192x312/14.26	75,000
072111.08	100	200	70	1	192 x 312/14.26	75,000
072611.03B	500	800	70	1/1	192 x 312/14.26	75,000
072211.01A	100	500	50	1/1	192 x 312/14.26	75,000
072211.07	500	800	50	1/1	192 x 312/14.26	75,000
072211.11	700	1400	50	1/1	192 x 312/14.26	75,000

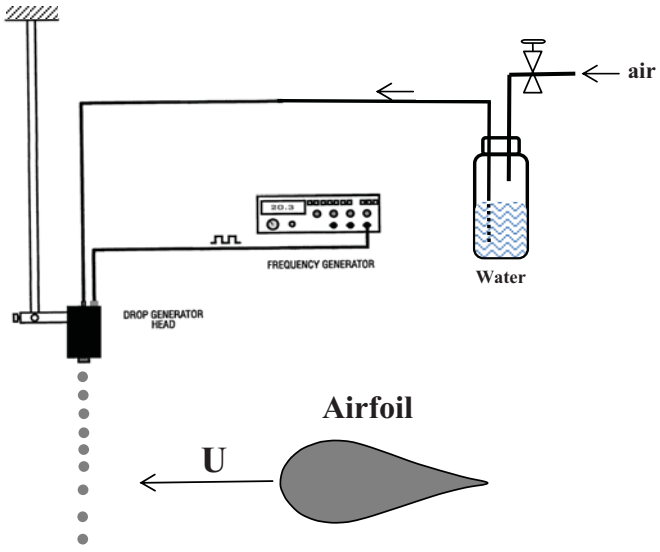

Figure 1. Conceptual View of the Experiment

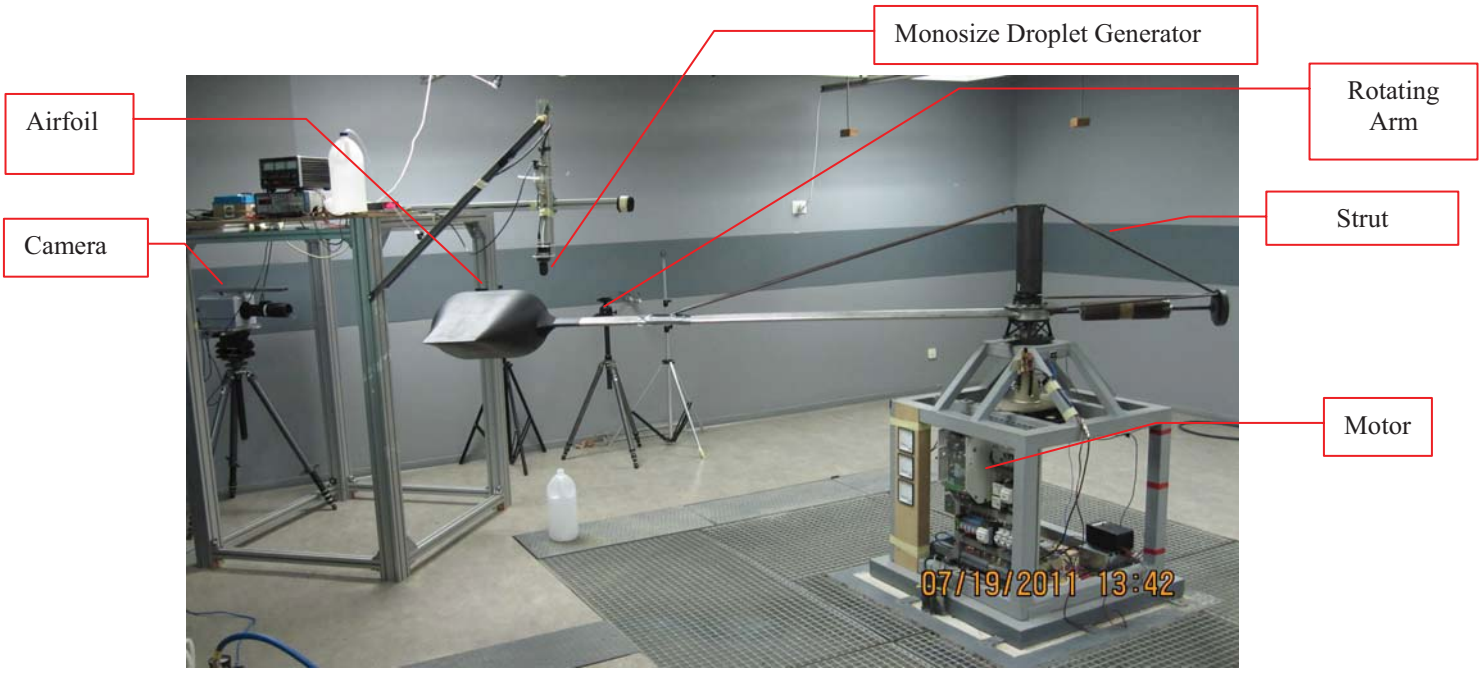

Figure 2. Experiment set-up in the INTA test cell

Figure 3. Close-up picture of airfoil (DBKUP 003, chord = 0.710 meters), TSI MDG-100 Monosize droplet generator and the high speed camera.

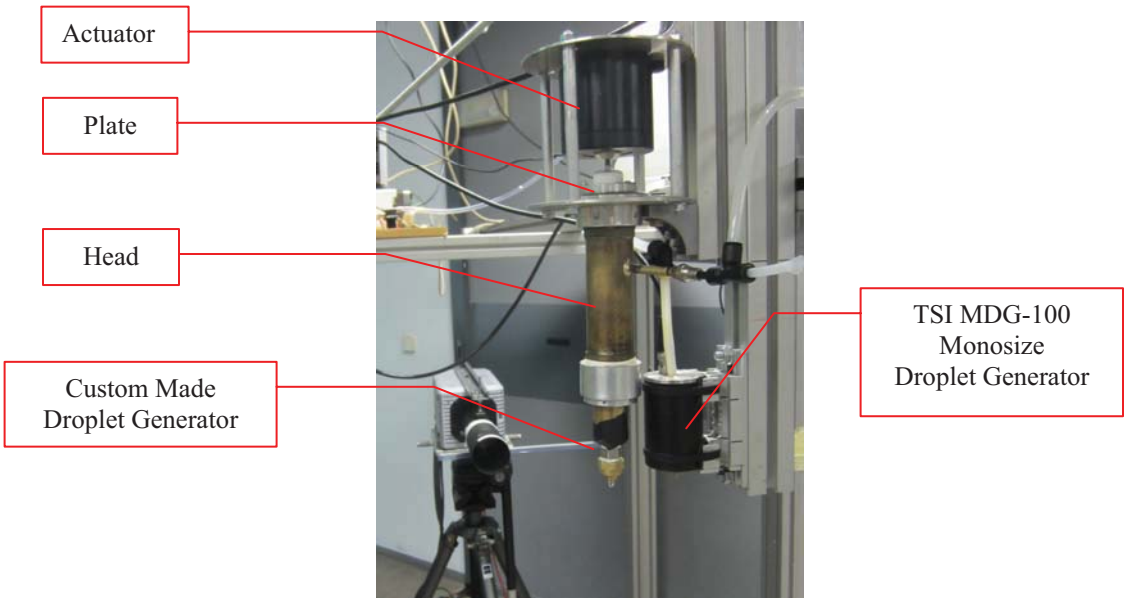

Figure 4. Droplet Generators TSI MDG-100 Monosize Droplet Generator is on the right side. On the left is the custom made droplet generator with its parts labeled.

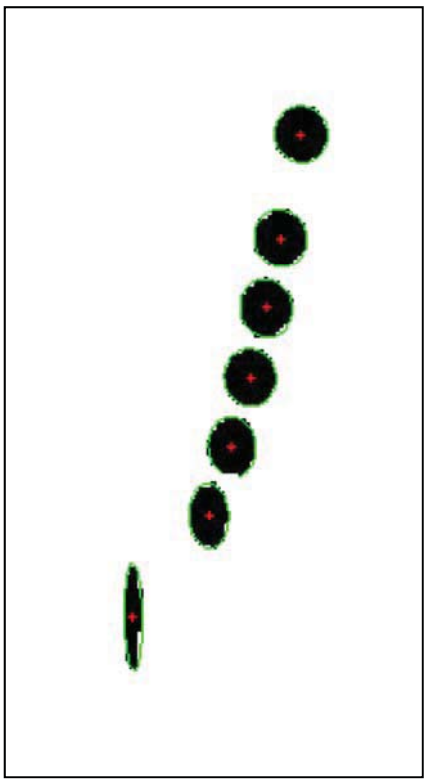

Figure 5. Sequence of droplet deformation with centroid and superimposed ellipse. Run 072011.11.5 droplet #1, droplet diameter = 903 μm, airfoil chord = 0.710 m, airfoil velocity = 80 m/sec. The location of the centroid is the red cross. The superimposed ellipse is plotted in green. The droplet is falling and moving from right to left.

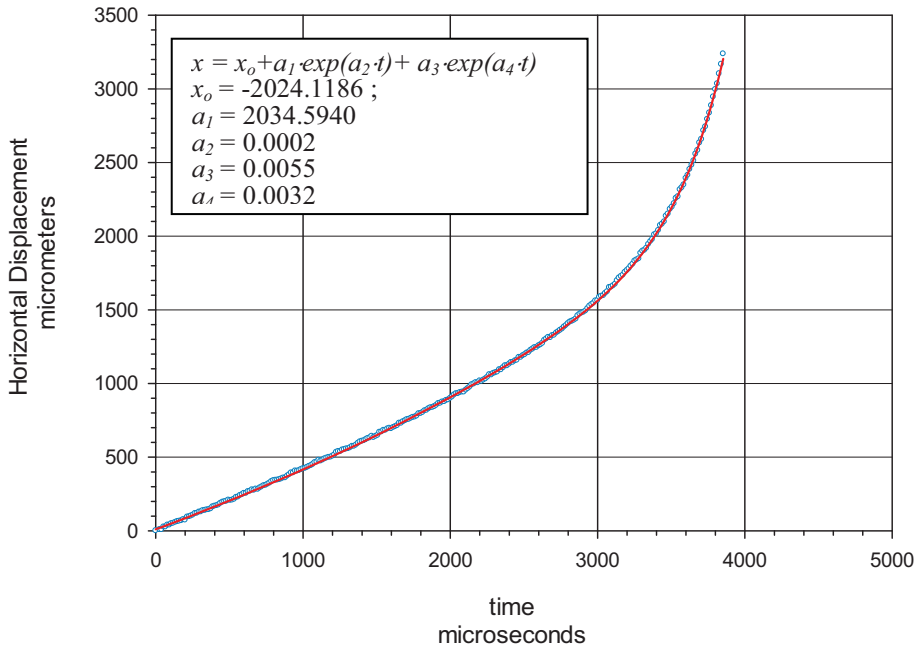

Figure 6. Horizontal Displacement against time. Run 072011.5 droplet #1, droplet diameter = 903 μm, airfoil chord = 0.710 m, airfoil velocity = 80 m/sec. Curve fit equation is indicated in the text box together with the curve fitting coefficients.

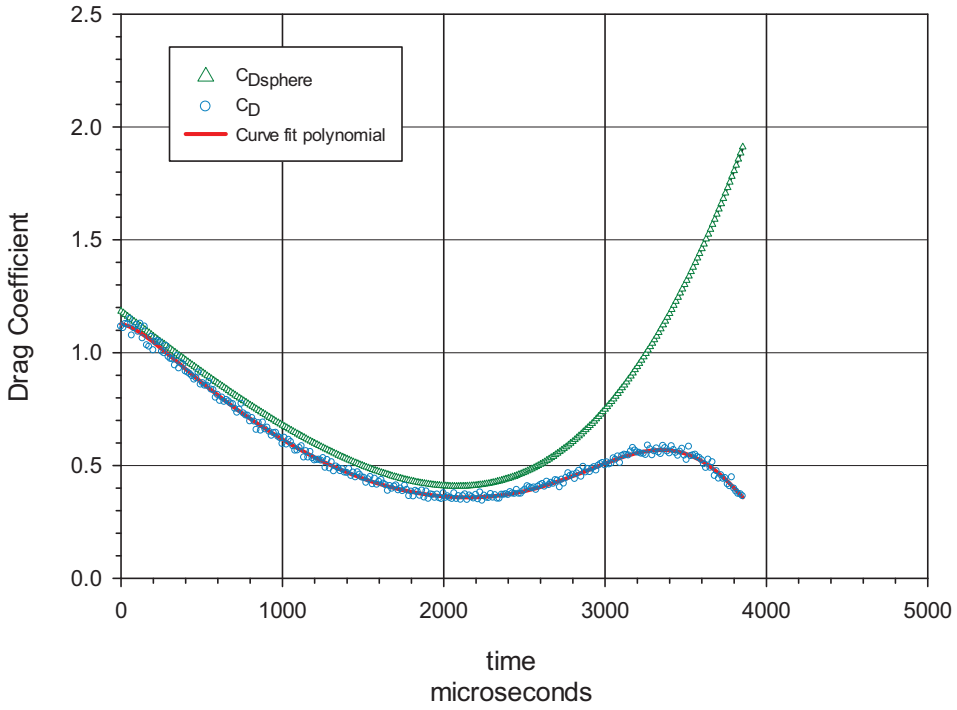

Figure 7. $C_{Dsphere}$ and C_D against time. Run 072011.5 droplet #1, droplet diameter = 903 μm, airfoil chord = 0.710 m, airfoil velocity = 80 m/sec. The data for C_D has been curve fitted with a polynomial to better indicate its trend.

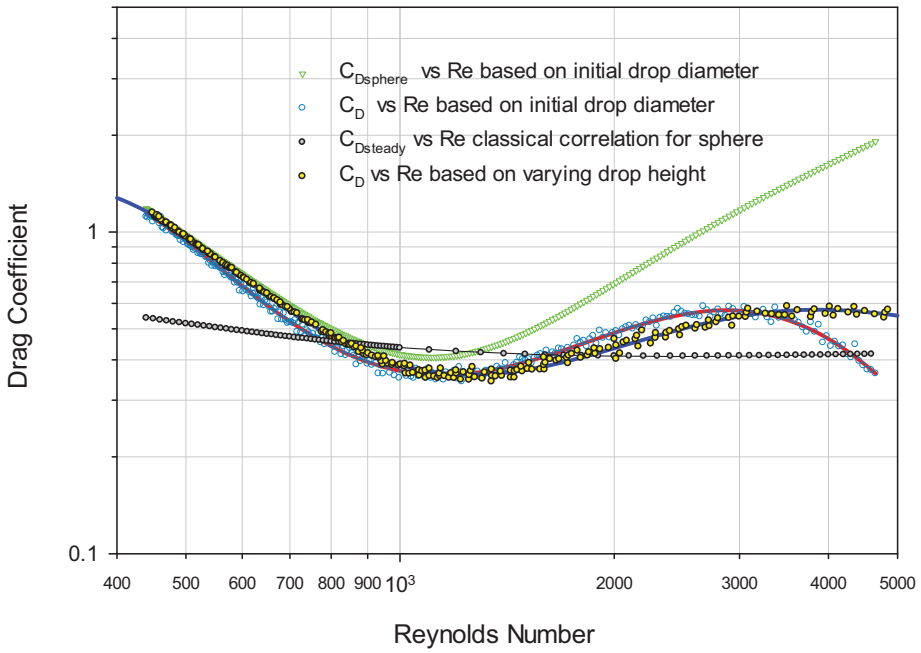

Figure 8. $C_{Dsphere}$, $C_{D\ and}$ $C_{Dsteady}$ against Reynolds Number. Run 072011.5 droplet #1, droplet diameter = 903 μm, airfoil chord = 0.710 m, airfoil velocity = 80 m/sec. $C_{Dsphere}$ vs. Re based on initial droplet diameter is in green triangles. C_D vs. Re based on constant droplet diameter is in white circles with blue edge, curve fitted with a red line. C_D vs. Re based on varying droplet height l(t) is in yellow circles with black edge, curve fitted with a blue line. $C_{Dsteady}$ vs. Re based on constant droplet diameter is the classical correlation for a sphere in steady state flow.

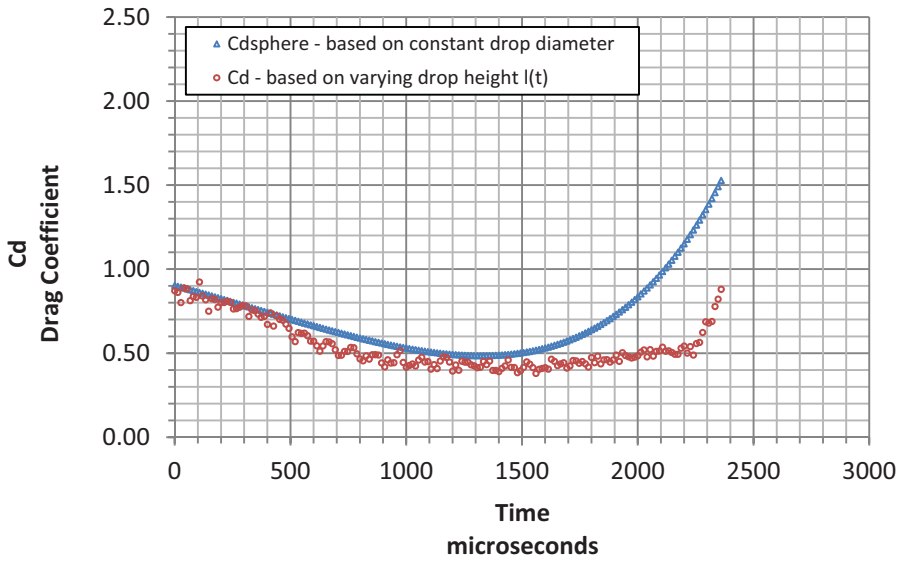

Figure 9. Drag Coefficient against Time. Run 072611.18.6 droplet #1, droplet diameter = 574 μm, airfoil chord = 0.710 m, airfoil velocity = 90 m/sec. The drag coefficient based on the initial droplet diameter (constant projected frontal area) is shown in blue. The drag coefficient based on the varying droplet height (variable projected frontal area) is shown in brown.

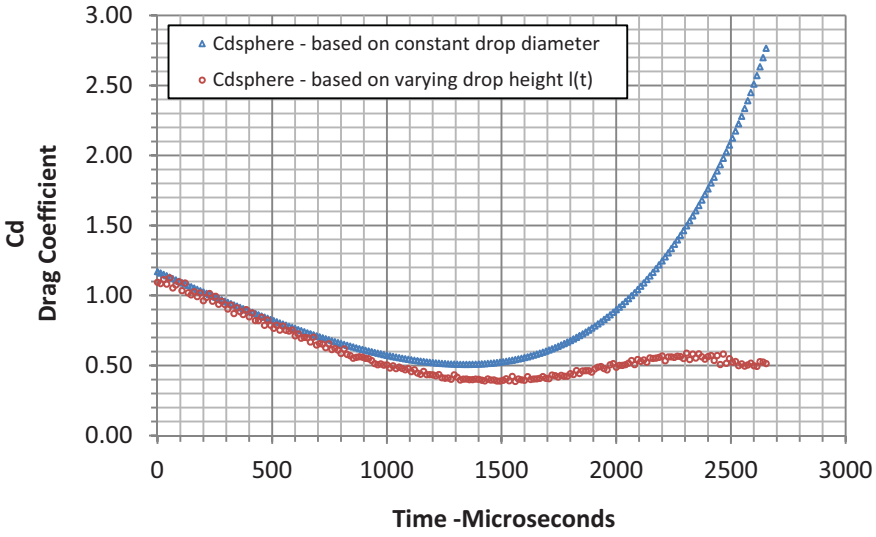

Figure 10. Drag Coefficient against Time. Run 072011.13A.1 drop #1, drop diameter = 1013 μm, airfoil chord = 0.710 m, airfoil velocity = 90 m/sec. The drag coefficient based on the initial droplet diameter (constant projected frontal area) is shown in blue. The drag coefficient based on the varying drop height (variable projected frontal area) is shown in brown.

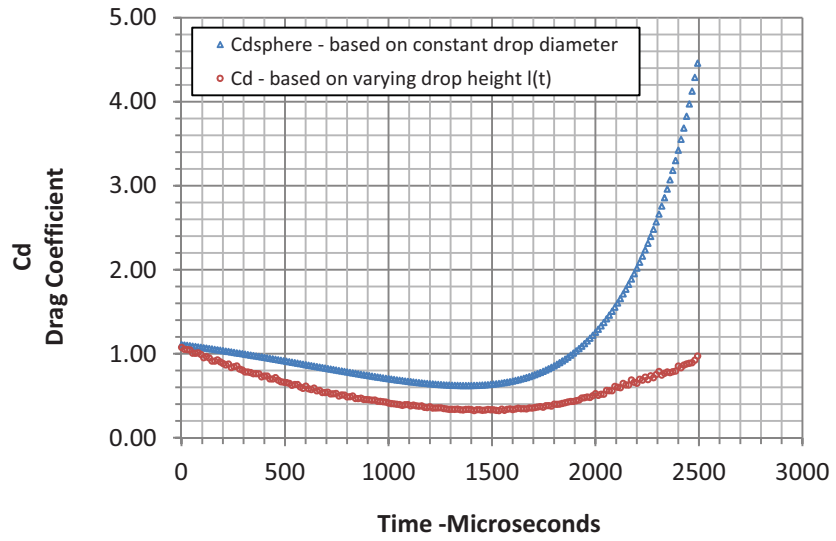

Figure 11. Drag Coefficient against Time. Run 072611.16.8 drop #4, drop diameter = 1271 μm, airfoil chord = 0.710 m, airfoil velocity = 90 m/sec. The drag coefficient based on the initial droplet diameter (constant projected frontal area) is shown in blue. The drag coefficient based on the varying drop height (variable projected frontal area) is shown in brown.

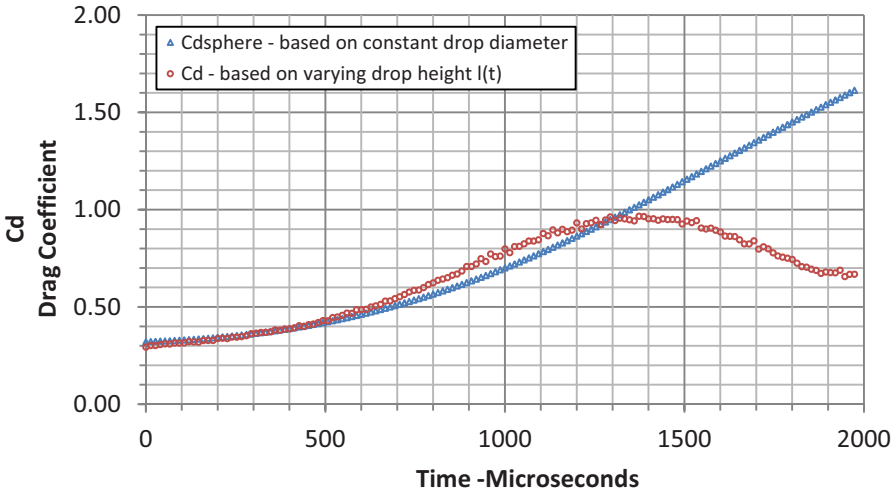

Figure 12. Drag Coefficient against Time. Run 072611.15B.10 drop #2, drop diameter = 1747 μm, airfoil chord = 0.710 m, airfoil velocity = 90 m/sec. The drag coefficient based on the initial droplet diameter (constant projected frontal area) is shown in blue. The drag coefficient based on the varying drop height (variable projected frontal area) is shown in brown.

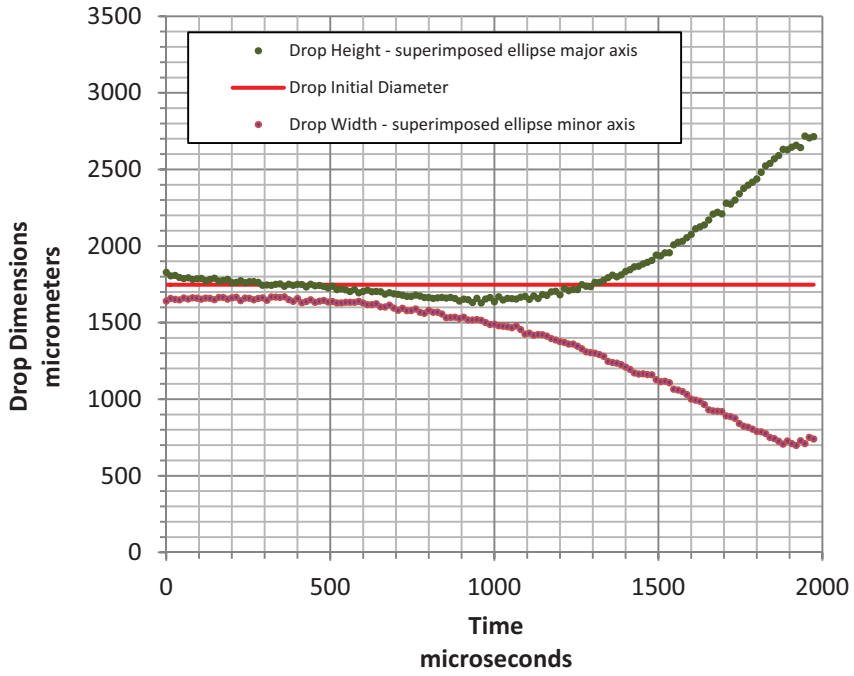

Figure 13. Droplet Oscillation showing in the Behavior of the Droplet Height, Width and Initial Diameter against Time. Run 072611.15B.10 drop #2, drop diameter = 1747 μm, airfoil chord = 0.710 m, airfoil velocity = 90 m/sec. The drop height is in green, the drop width is in purple and the drop original diameter is in red.

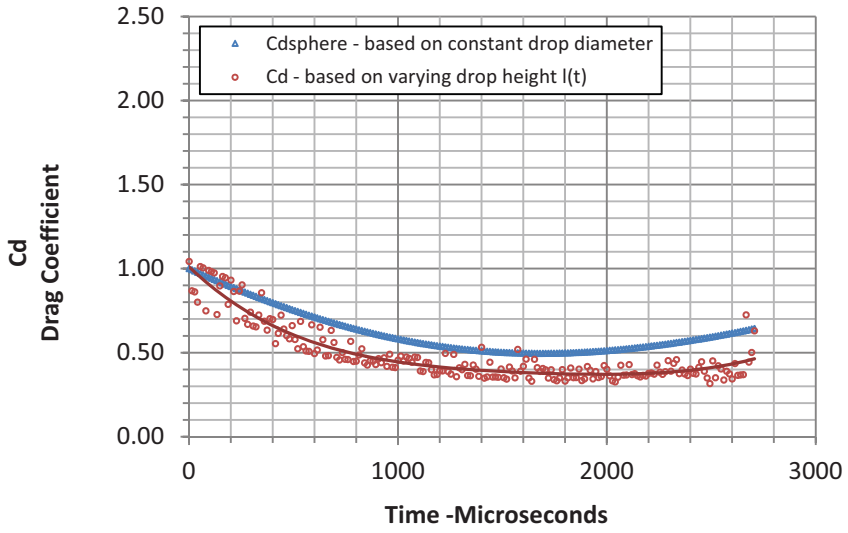

Figure 14. Drag Coefficient against Time. Run 072111.8.3 drop #10, drop diameter = 321 μm, airfoil chord = 0.710 m, airfoil velocity = 70 m/sec. The drag coefficient based on the initial droplet diameter (constant projected frontal area) is shown in blue . The drag coefficient based on the varying drop height (variable projected frontal area) is shown in brown. Data for C_{d3} is curve fitted with a fourth degree polynomial.

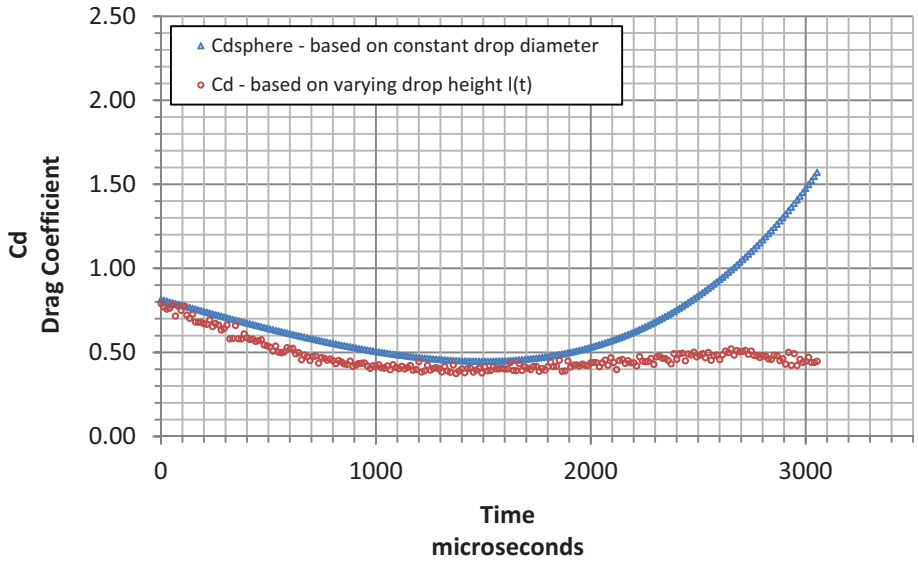

Figure 15. Drag Coefficient against Time. Run 072611.3B.10 drop #2, drop diameter = 720 μm, airfoil chord = 0.710 m, airfoil velocity = 70 m/sec. The drag coefficient based on the initial droplet diameter (constant projected frontal area) is shown in blue. The drag coefficient based on the varying drop height (variable projected frontal area) is shown in brown.

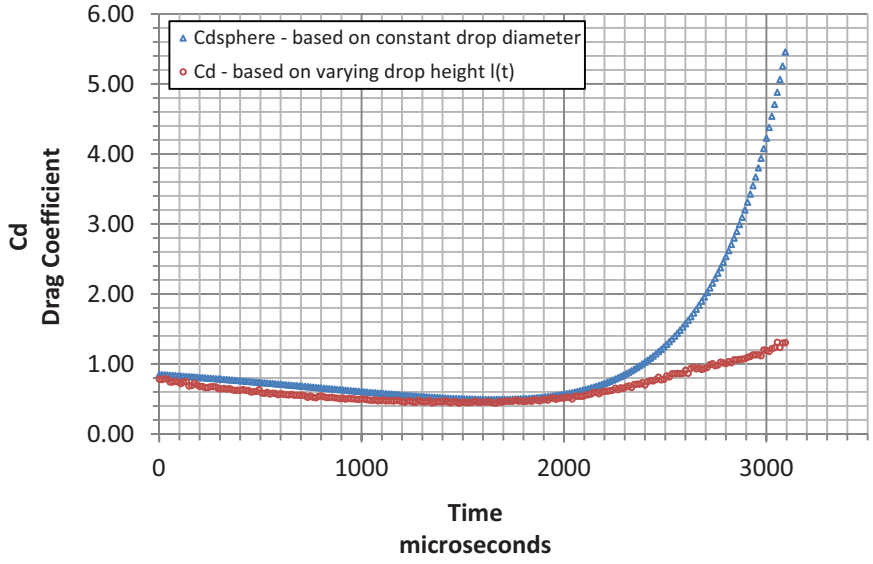

Figure 16. Drag Coefficient against Time. Run 072611.3B.1 drop #7, drop diameter = 1096 μm, airfoil chord = 0.710 m, airfoil velocity = 70 m/sec. The drag coefficient based on the initial droplet diameter (constant projected frontal area) is shown in blue . The drag coefficient based on the varying drop height (variable projected frontal area) is shown in brown.

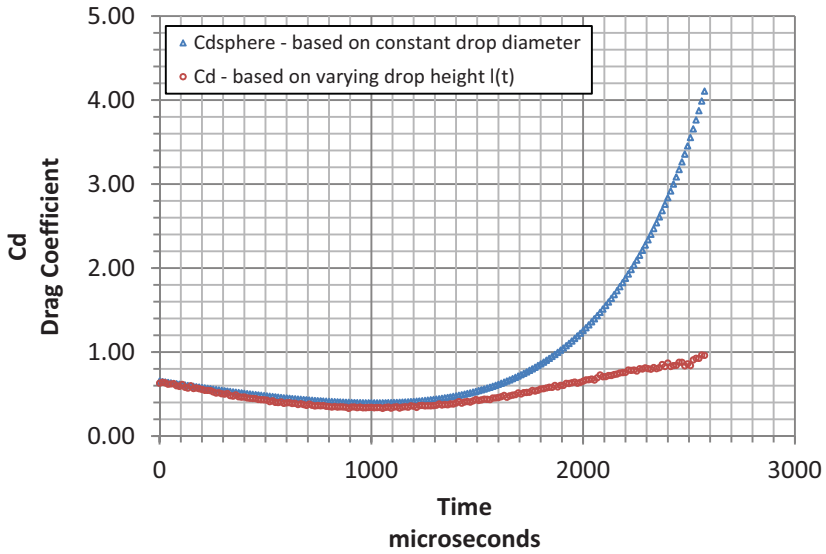

Figure 17. Drag Coefficient against Time. Run 072611.3B.3 drop #3, drop diameter = 1308 μm, airfoil chord = 0.710 m, airfoil velocity = 70 m/sec. The drag coefficient based on the initial droplet diameter (constant projected frontal area) is shown in blue. The drag coefficient based on the varying drop height (variable projected frontal area) is shown in brown..

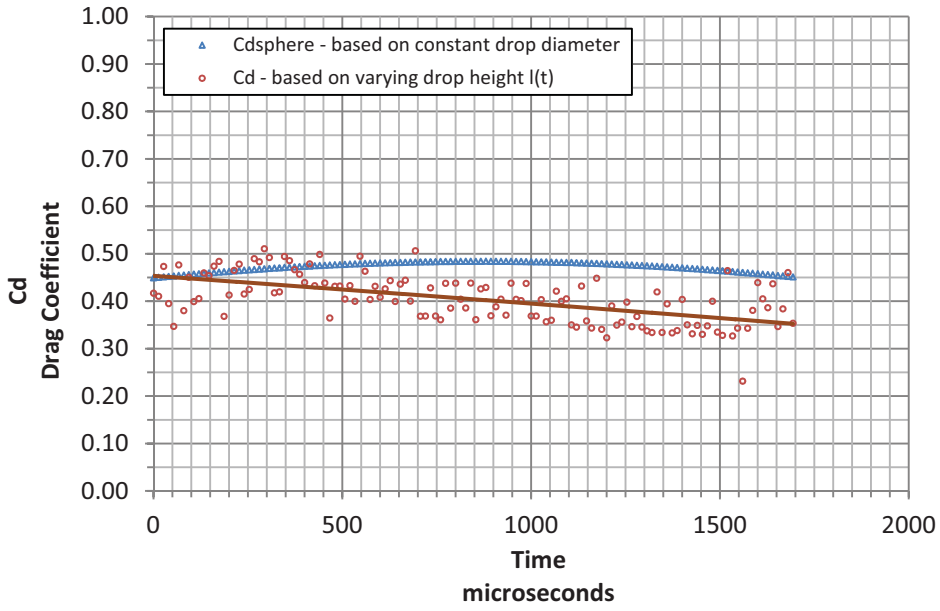

Figure 18. Drag Coefficient against Time. Run 072211.1.8 drop #6, drop diameter = 375 μm, airfoil chord = 0.710 m, airfoil velocity = 50 m/sec. The drag coefficient based on the initial droplet diameter (constant projected frontal area) is shown in blue. The drag coefficient based on the varying drop height (variable projected frontal area) is shown in brown.

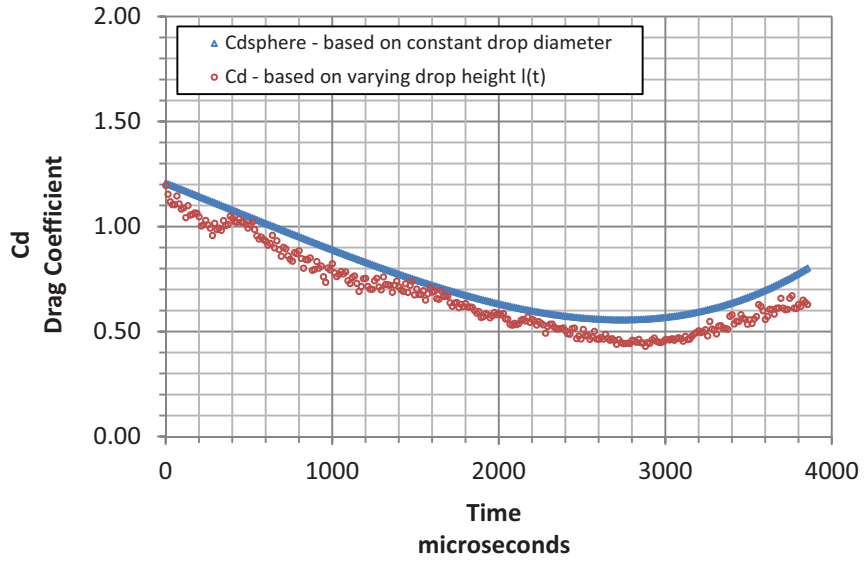

Figure 19. Drag Coefficient against Time. Run 072211.7.1 drop #10, drop diameter = 779 μm, airfoil chord = 0.710 m, airfoil velocity = 50 m/sec. The drag coefficient based on the initial droplet diameter (constant projected frontal area) is shown in blue. The drag coefficient based on the varying drop height (variable projected frontal area) is shown in brown.

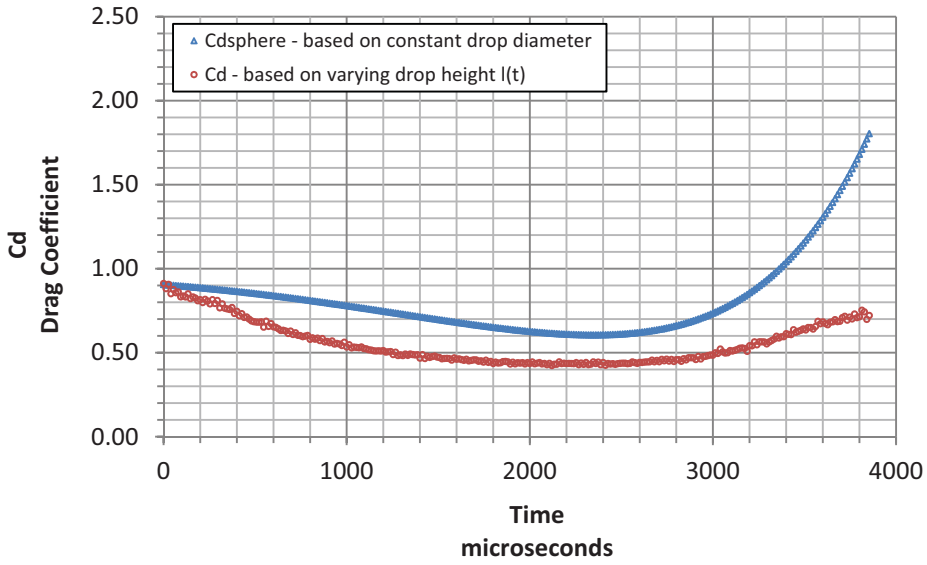

Figure 20. Drag Coefficient against Time. Run 072211.11.2 drop #3, drop diameter = 1270 μm, airfoil chord = 0.710 m, airfoil velocity = 50 m/sec. The drag coefficient based on the initial droplet diameter (constant projected frontal area) is shown in blue. The drag coefficient based on the varying drop height (variable projected frontal area) is shown in brown.

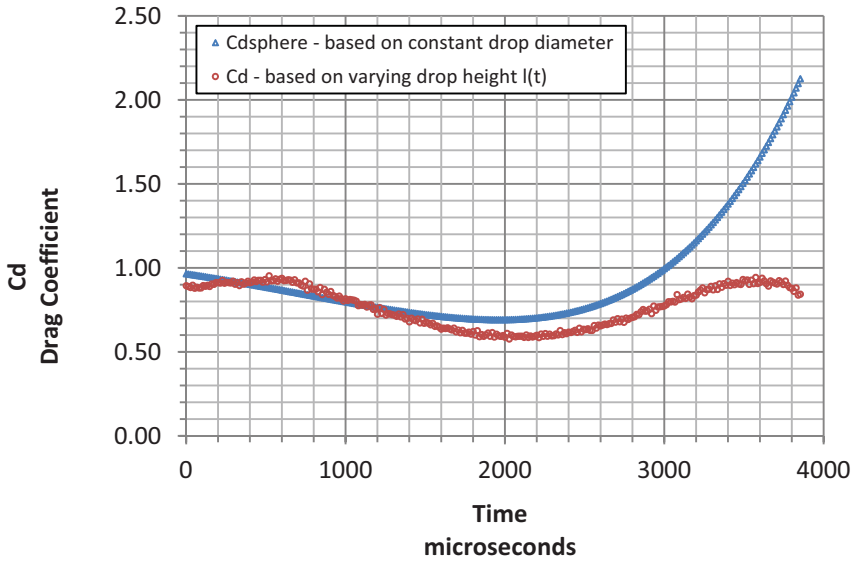

Figure 21. Drag Coefficient against Time. Run 072211.11.3 drop #3, drop diameter = 1433 μm, airfoil chord = 0.710 m, airfoil velocity = 50 m/sec. The drag coefficient based on the initial droplet diameter (constant projected frontal area) is shown in blue. The drag coefficient based on the varying drop height (variable projected frontal area) is shown in brown.